Fully Two-Dimensional Particle-In-Cell Monte Carlo Collisions Model of a Wall-Less Hall Thruster

IEPC-2015-311／ISTS-2015-b-311

Presented at Joint Conference of 30th International Symposium on Space Technology and Science
34th International Electric Propulsion Conference and 6th Nano-satellite Symposium,
Hyogo-Kobe, Japan
July 4 – 10, 2015

L.Garrigues[1]
LAPLACE (Laboratoire Plasma et Conversion d'Energie),
Université de Toulouse, UPS, INPT Toulouse
118, route de Narbonne, F-31062 Toulouse cedex 9, France
CNRS; LAPLACE; F-31062 Toulouse, France

S. Mazouffre[2], J. Vaudolon[3], and S. Tsikata[4]
ICARE (Institut de Combustion Aérothermique Réactivité et Environnement),
1C Avenue de la Recherche Scientifique, F-45071 Orléans cedex 2, France

A new Hall thruster configuration has been proposed to prevent ions bombardment on ceramic walls to increase thruster lifetime. The specificity of the wall less Hall thruster configuration is related to the position of the anode that is shifted in the exhaust plane. A two-dimensional Particle-In-Cell Monte Carlo Collisions model is used to describe plasma properties. Calculation results show that similar behavior as for standard configuration is achieved with strong current oscillations in the range of tens of kHz due to breathing mode instability and MHz instability related to electron cyclotron instability responsible for cross magnetic field electron transport. A loss in acceleration efficiency is observed due to overlap between ionization and acceleration layers, as in experimental results.

Nomenclature

roman characters

B	=	magnetic field strength (T)
B_z	=	radial magnetic field strength (T)
d	=	length in azimuthal direction (m)
e	=	electron charge constant (1.6×10^{-19} C)
E_x	=	axial electric field (V. m^{-1})
E_y	=	azimuthal electric field (V. m^{-1})
E_{yf}	=	fluctuating azimuthal electric field (V. m^{-1})
k_B	=	Boltzmann constant (1.38×10^{-23} JK^{-1})
k_y	=	Wave number (m^{-1})

[1] Senior Scientist at CNRS, laurent.garrigues@laplace.univ-tlse.fr.
[2] Senior Scientist at CNRS, stephane.mazouffre@cnrs-orleans.fr.
[3] Ph.D. candidate, julien.vaudolon@cnrs-orleans.fr.
[4] Scientist at CNRS, sedina.tsikata@cnrs-orleans.fr.

L	=	length is axial direction (m)
m_e	=	electron mass (kg)
n_e	=	plasma number density (m^{-3})
t	=	time (s)
T_e	=	electron temperature (K)
V_a	=	applied electric potential (V)
V_d	=	azimuthal electron drift velocity ($m.s^{-1}$)
x	=	axial direction (m)
y	=	azimuthal direction (m)
z	=	radial direction (m)

greek characters

α	=	scaling factor
Δt	=	time step (s)
Δx	=	axial grid spacing (m)
Δy	=	azimuthal grid spacing (m)
ε_0	=	vacuum permittivity (8.85×10^{-12} $F.m^{-1}$)
λ	=	wavelength (m)
λ_d	=	Debye length (m)
ω_c	=	electron cyclotron frequency (s^{-1})
ω_p	=	electron plasma frequency (s^{-1})

I. Introduction

In a Hall Thruster (HT), a discharge is ignited in a crossed magnetic and electric fields configuration inside an annular ceramic channel. The anode is situated at the rear of the device through which the xenon gas is injected. An electron-emitting hollow cathode is placed downstream of the channel. A discharge voltage applied between the anode and the cathode is responsible for the almost axial acceleration of the ions and the engine thrust. In such a conventional thruster, the ionization of the neutral gas occurs inside the channel. If most of ions are accelerated towards outside of the thruster, a fraction of us bombards the ceramic walls close the channel exhaust, resulting in wall erosion that reduces the thruster lifetime [1].

The origin of such drawback is related to the HT magnetic field configuration. The magnetic field is generated by one internal and four external magnetic coils. An appropriate magnetic circuit leads to a converging magnetic lens. In a first approximation, the lines of magnetic force tend to be equipotential. In the exhaust plane, where the maximum strength of magnetic field is located, the magnetic field has a component mainly in the radial direction. Electrons are drifting in the azimuthal direction under axial electric and radial magnetic fields. In the axial direction, because the electron motion is impeded by the imposed magnetic field, the electric field penetrates giving rise to a large electron temperature localized close to the thruster exit. The equipotential lines then deviate from the magnetic field lines inducing a loss of ions on the walls [2]. Different solutions have been identified/considered: 1) new ceramics or new procedure of ceramics fabrication with a higher resistance to erosion, 2) new design of ceramic walls with a conical shape at the end (deduced from ceramic shape after ending endurance lifetime [3]), 3) new magnetic field configurations to prevent erosion of the thruster channel walls by reducing the plasma-surface interactions [4-5]. A new design of a HT has then been proposed combining new designs of channel walls and magnetic field topology [6-8]. In the proposed magnetic field topology called magnetic shielding, the magnetic field lines close to the channel walls are now in the axial direction almost parallel to the walls that makes easy the motion of trapped electrons from the outer and inner magnetic poles to the anode region and vice versa. As a consequence, close to the walls, the electron temperature is reduced, the electric potential drop along the magnetic field lines becomes negligible, and magnetic field lines tend to be equipotential. Ions are focused in the direction of the center of the channel, preventing impacts on the channel walls.

The issue of erosion and losses on walls is more challenging for small and low power HTs because the surface/volume is less favorable when the size scales down and the miniaturization of the thruster offers less flexibility in term of magnetic field topology variation. A new concept called “Wall Less Hall Thruster” WLHT has been recently proposed and tested [9]. In this concept, channel walls no longer play a role because the anode is positioned in the exit plane of the thruster and the discharge occurs outside of the engine. Note that this concept is not only dedicated to small size engine. The objective of this paper is to use a two-dimensional Particle-In-Cell (PIC) model with Monte-Carlo Collisions to study the plasma properties. The rest of the paper is organized as the following. We describe in section II the WLHT prototype, while the basics of PIC model are reported in section III. Section IV is dedicated to modeling results. We summarize our main results in section V.

II. Description of WLHT prototype and recent experimental results

A schema and a photo of the WLHT are presented in Figure 1. In conventional HT, the anode plane through which the neutral gas is injected is placed at the rear of the channel. In the WLHT, as we note in figure 1, the anode is separated from the gas injection and placed in the channel exit. The magnetic field is established with permanent SmCo magnets positioned above (respectively below) the outer (respectively inner) ceramic walls. A magnetic circuit made in soft iron permits to design the desired magnetic field topology, meanwhile the number of magnets permits to change the magnetic field strength as wanted. The ceramic walls are made in $BNSiO_2$. The width of the channel can be easily modified by changing the diameter of the ceramics [10]. The WLHT has been characterized in the NExET (New Experiments on Electric Thrusters) vacuum chamber. The backpressure is on the order of $2x10^{-5}$ Torr in xenon for a xenon mass flow on the order of 1 $mg.s^{-1}$.

(a) (b)

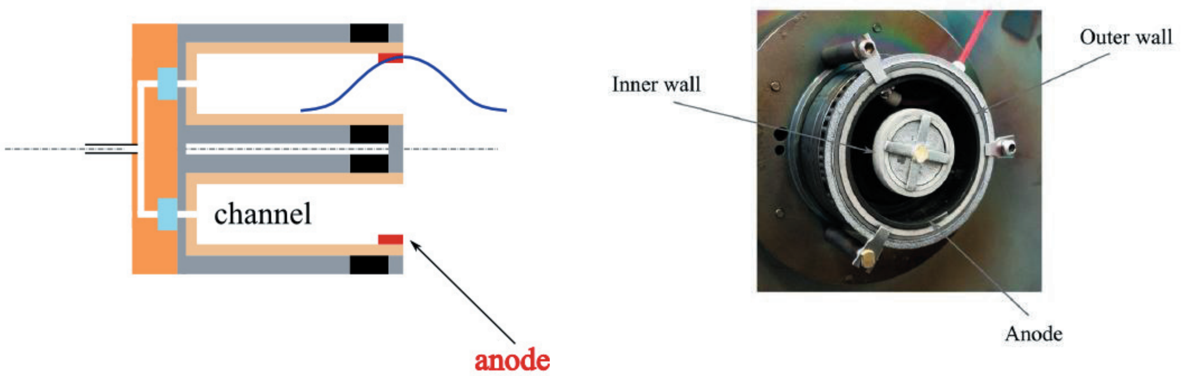

Figure 1. (a) Schema, (b) photo of the WLHT without the cathode [9].

(a) (b)

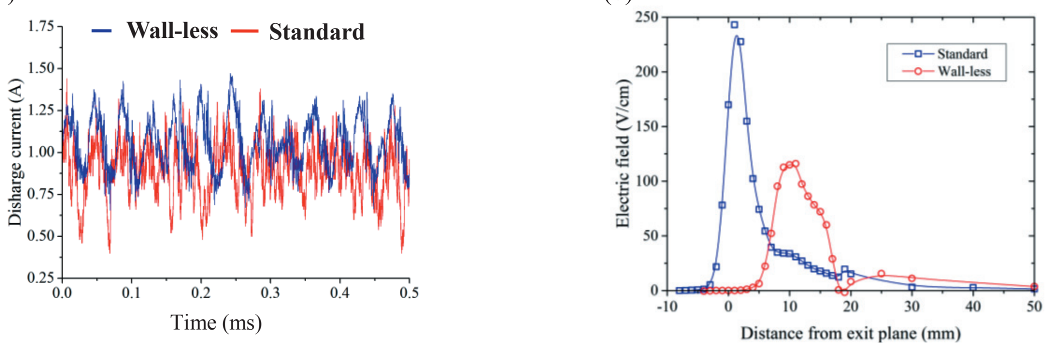

Figure 2. (a) Discharge current oscillations, (b) electric field profile in the standard and wall-less configuration [9]. The applied voltage is 200 V and the xenon mass flow is 1 $mg.s^{-1}$.

Current-voltage characteristics for varying xenon mass flow rates and voltages are presented in Ref. [9]. The variation of discharge current as a function of time exhibits breathing mode oscillations at a frequency between 20 and 25 kHz, as in HTs, as we see in Fig. 2a. Ion velocity profile has also been measured by means of Laser-Induced Fluorescence (LIF) technique showing that the acceleration of ions occurs 15 mm downstream the exit plane, in the very near plume of the engine (see Fig. 2b). Indirect measurements seem to show that the ionization mainly takes place also in the near plume. First experimental campaigns show that a stable regime can be achieved with the WLHT prototype where plasma surface interactions are reduced. Nevertheless, some drawbacks exist; e. g. the discharge current seems larger than the one measured in HT for same conditions. Efforts are now directed to optimize the thruster parameters.

III. Description of the PIC MCC model

The electrostatic PIC model permits a statistical representation of the distribution functions of charged particles under electric and magnetic fields influence and electron-neutral collisions, the effect of the space charge on the electric field profile being calculated through Poisson equation. We assume that the magnetic field is not modified by the plasma. Ionization and elastic collisions between electrons and atoms are taken into account with a Monte Carlo method with a null collision technique. In this work, the two-dimensional PIC model describes the azimuthal and axial directions, named y and x in the rest of paper, respectively (see Figure 3). We discard the radial direction z. To reduce computational time only a sector of 1 cm length in the azimuthal direction is described, periodic conditions at y = 0 and y = d are then used for particles and electric potential. In the axial direction, the anode is fixed at x = 0 and the model ends at x = L cm where the cathode plane is positioned. An explicit leap frog schema is used to integrate charged particle trajectories [11-12]. Because the mass of the ions is large, only electrons feel the magnetic field influence. The magnetic field perpendicular to the simulation domain is in the z direction. The profile of magnetic field along the x direction is also shown in Fig. 2. Electrons and ions passing the anode and cathode planes are removed from the simulation domain. The injection of electrons at x = L is calculated through a balance of charged particles between anode and cathode planes. The energy distribution of new injected electrons is sampled from a Maxwellian energy distribution with a temperature of 1 eV. We assume that no ionization takes place inside the channel, atoms are then injected in the anode plane with an initial density of $2\text{x}10^{19}$ m^{-3} at x = 0 and a one-dimensional fluid equation is used to model their transport. The electric potential is fixed to V_d at x = 0 and at 0 V at x = L. PARDISO (Parallel Sparse Direct Linear Solver) is used to solve the Poisson equation [13-14].

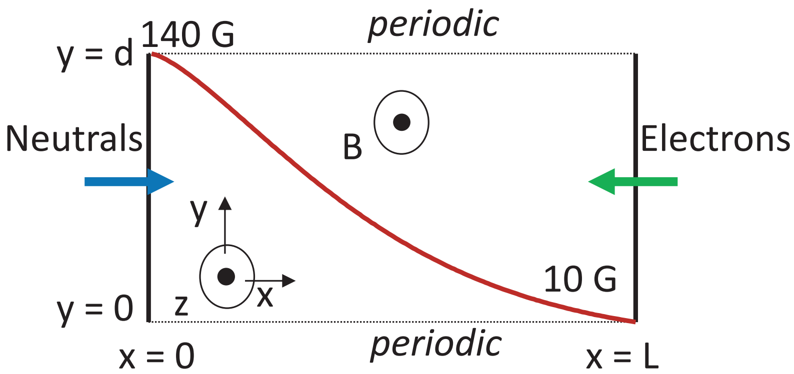

Figure 3. Two dimensional computational domain [(x,y) plane], the axial profile of the magnetic field (perpendicular to the simulation domain in the z direction) is also shown. The position of the exhaust plane is at x = 0 where V = V_a, at x = L, V = 0 V. The dimensions of the computational domain are d = 1 cm and L = 2 cm.

Severe constrains about time step Δt (Δt < $0.2/\omega_p$, $\omega_p = \sqrt{e^2 n_e / m_e \varepsilon_O}$ being the electron plasma frequency) and mesh grid size Δx,y (Δx,y < λ_d, $\lambda_d = \sqrt{k_B T_e / e^2 n_e}$ being the electron Debye length) exist for explicit PIC scheme. For typical plasma density on the order of 10^{18} m^{-3} and electron temperature of few tens of eV as in HTs, 10^5 mesh grid points would be needed for a domain of 2 cm long and 1 cm large, along with a time step Δt on the order of 3×10^{-12} s. To overcome such constraints, a scaling method that consists to increase the vacuum permittivity by a scaling factor α greater than 1 has successfully been used [15-17]. In this study, the scaling factor α is fixed to 20; the number of grid points is 200 and 100 in x and y directions, respectively. Constrain about time step according to the plasma frequency limitation can be relieved. Nevertheless, because micro-turbulence with a short wavelength on the scale of Larmor radius has to be resolved, the electron cyclotron frequency ω_c ($\omega_c = eB/m_e$) has still to be solved during electron motion [18-19]. The total number of macro-particles (electrons and ions) is around 600 by cells. Also to reduce the computational time to typically one week for a bi-processor with six cores machine, we employ a hybrid parallel programing technique with distributed and shared memories combining OpenMP (Open Multi-Processing) and MPI (Message Passing Interface) standards. More details about the model description and techniques can be found in Ref. 20.

IV. Results and discussion

Calculations have been performed for V_a = 300 V and a neutral density at x = 0 of 2x10^{19} m^{-3}. We have reported in figure 4 the transient evolution of the ion current at the end of the simulation domain and two dimensional – time and x position - profiles of neutral and ion densities and axial electric field (profiles have been averaged along the y direction). Strong current oscillations at a frequency twice that the one measured appear. Note that preliminary results with a reduced magnetic field gradient for a same maximum of 140 G exhibits less intense current oscillations with a lower frequency more close to experimental results (not shown). The analysis of neutral and ion density profiles in Figures 4b and 4c show that the ionization takes place 5 mm downstream of the exhaust plane. The maximum of plasma density (2.2x10^{18} m^{-3}) at t = 12 µs is obviously correlated to the position of the front of neutral atoms. Numbers of studies with hybrid [2], [21], fluid [22], and PIC models [18], [20] detail the breathing mode of neutral atoms. The two-dimensional hybrid and fluid approaches describe the radial and axial directions and "anomalous" cross-magnetic field electron transport induced by non-collisional transport must be assumed. Instead of the two-dimensional azimuthal-axial PIC models, as in this study, no "anomalous" electron transport is assumed; we will analyze the mechanism responsible for electron transport further in the paper. In figure 4c, we see that the axial electric field profile also oscillates as a function of time. When the ion current is minimum the axial electric field concentrates between x = 0.5 and 1 cm (corresponding roughly to the acceleration region), at the opposite, when the ion current is maximum, the acceleration region extends on 5 mm close to x = 0.

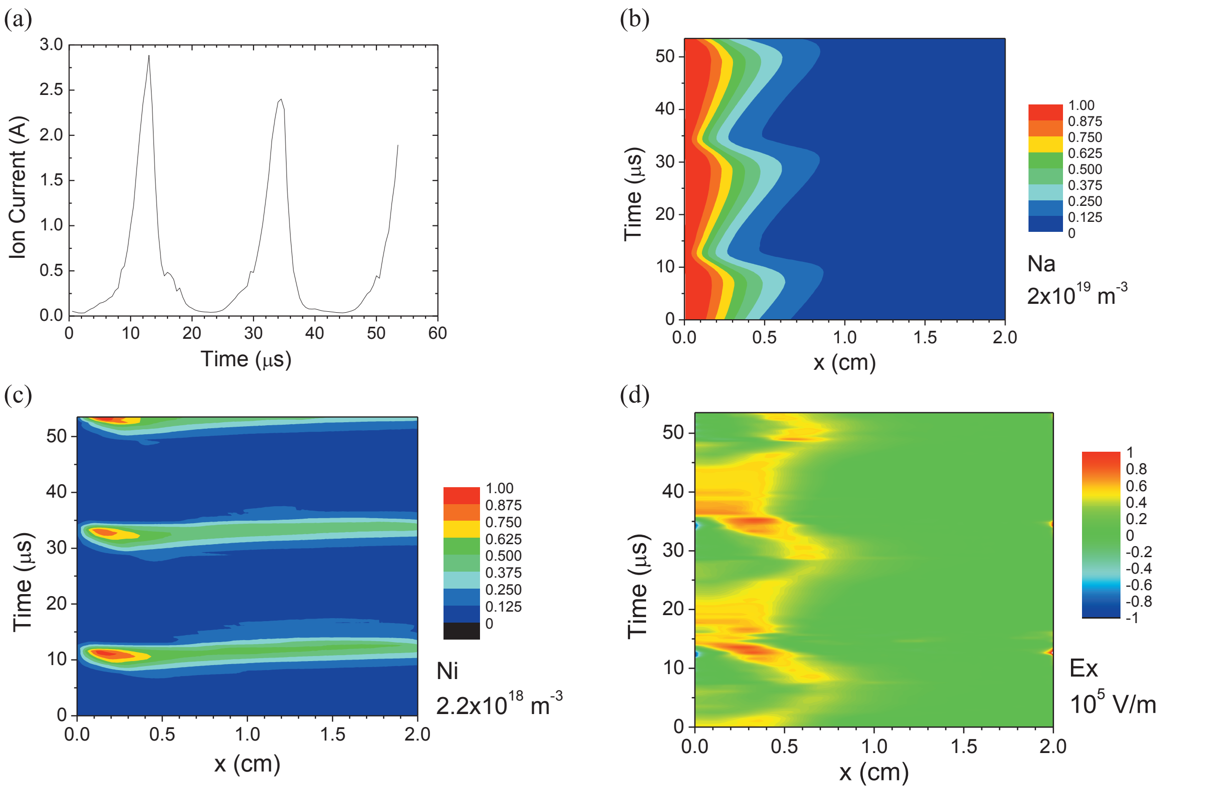

Figure 4. (a) Ion current recorded at L = 2 cm, two dimensional profiles: (b) neutral density, (c) ion density, and (d) axial electric field averaged along the y direction.

The time-averaged axial electric field profile is shown in Figure 5 together with the axial ion velocity profile. The maximum of electric potential averaged in time reaches 400 V/cm, that is larger than the measured one but for an applied potential of 200 V. In the experimental results, the acceleration region thickness extends on 1.5 cm while the same acceleration region is concentrated on 1 cm length in the calculations. Most of the ions win their final velocity around 12 km/s at x = 1 cm. Ions created close to the x = 0 plane are accelerated towards it, the sign of the axial ion velocity changes of sign at x = 0.1 cm. Most interesting, if we calculate the maximum of velocity obtained by an ion of almost zero initial velocity with an applied voltage of 300 V one finds 21 km/s. The loss in acceleration efficiency is due to the overlap between ionization and acceleration regions.

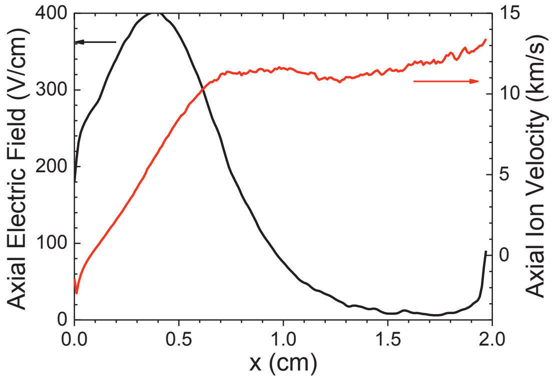

Figure 5. Axial electric field and ion velocity profiles averaged along the y direction and time.

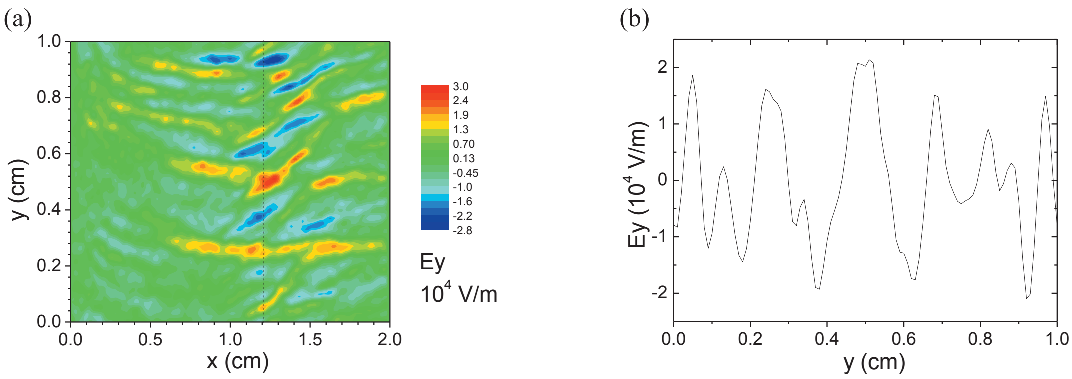

Figure 6. (a) Two dimensional profile (axial and azimuthal directions) of azimuthal electric field, (b) one dimensional profile of azimuthal electric field at x = 1.2 cm (along the dotted line of Figure a). The time is t = 53 µs.

Due to the intense ionization of the neutral gas, when the ion current becomes large, the origin of the "anomalous" mechanism that is able for electrons to pass the localized magnetic field layer has to be addressed. The question of electrostatic waves for magnetized and Maxwellian electrons, and unmagnetized and collisionless ions, has been theoretically studied in Ref. 23 and completed in Ref. 24 by Gary and Sanderson, originally. An extension can be found in [19]. The solution of dispersion relation shows that an electron cyclotron instability induced by the coupling between ion acoustic waves and electron Bernstein modes occurs in the ExB drift direction corresponding to the y direction in our simulation. The discrete wave number k_y is given by:

$$k_y = n\frac{\omega_c}{V_d} \quad (1),$$

Where V_d is the azimuthal electron drift velocity ($V_d = E_x/B_z$) and n is an integer greater than 1. For typical conditions a magnetic field of 100 G and an axial electric field of 4×10^4 V.m^{-1}, one find wave number k_y on the order of 500 m^{-1} and a wavelength λ about 2 mm that corresponds to the Larmor radius. We have plotted in Figure 5a the two-dimensional profile of azimuthal electric field E_y at a time t = 53 µs. We see that the instability obtained with the model is closely linked to the one predicted by the theory. It obviously been observed for conventional HTs with two-dimensional PIC models [18-20] and measured through a coherent Thomson scattering technique [25]. Nevertheless, the profile of E_y exhibits more than one mode (see Figure 6b); a detailed shows that analysis the signal is composed with a multitude of modes with different amplitudes.

The other question related to effect of this instability on electron transport. Some analogy with the heating of ions in Tokamak discharges by lower hybrid wave obtained by Karney [26] has been proposed by Adam and co-workers to explain electrons heating and transport in HTs [18], [19]. In the x direction, when collisional mechanism occurs, old velocity components are changed in new components and electrons change of magnetic field lines. When an electron interacts with a wave, the electron oscillates during one gyration period. Oscillations caused by the wave disturbances remain linear as the electron and the wave does not have the same velocity. When the electron and the wave have same velocity a resonance occurs and the electron trajectory becomes stochastic if the ratio between fluctuating azimuthal and axial electric fields is larger than a given threshold depending on $k_y V_d / \omega_c$ [19], [27]. Typically electron drift velocity of 4x10^6 m.s^{-1} gives energy of 45 eV, only the population of the tail of the electron energy distribution is concerned. The fluctuating azimuthal electric field E_{yf} ($E_{yf} = \sqrt{\langle E_y^2 \rangle}$ – the brackets indicating averaged values) has been calculated. We have plotted in Figure 7 the two-dimensional profile of E_{yf} (x direction and time – averaged along y direction). The effect of fluctuating electric field on electron transport is obvious; the larger the E_{yf} the larger the electron current at the anode. The fluctuating electric field becomes negligible when the current is close to zero (see Figure 2a). We also notice that the positions of the maximum of E_{yf} and E_x (shown in Figure 4d) are correlated in time (as expected) but not in position. The ion transport in the direction of the cathode is certainly responsible of this effect. If we compare the amplitude of E_{yf} and E_x, we see that the amplitude of E_{yf} only represents in averaged around 10 % of E_x. It seems that the conditions for stochastic electron trajectories mentioned above are not fulfilled (almost in average). Nevertheless, the presence of the wave induces disturbances modify electron trajectories leading to an increase of the Larmor radius, as it was recently observed with one-dimensional PIC simulation [28].

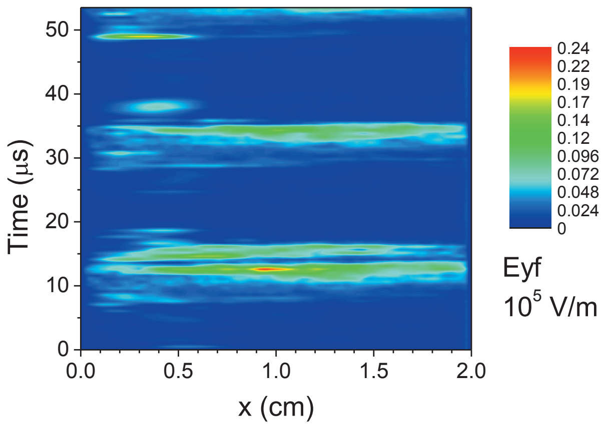

Figure 7. Two dimensional profile (axial direction and time – averaged along the azimuthal direction) of fluctuating azimuthal electric field. Same scale as in Figure 2d is used.

V. Conclusion

A new HT configuration called WLHT has been proposed to increase thruster lifetime, especially for low power engines. In the WLHT configuration, the injection of gas is separated from the anode that is positioned at the exhaust, the ion acceleration occurs outside of the thruster, in the negative gradient of the magnetic field profile. This new configuration offers also more possibility to use diagnostics to characterize plasma properties. We have used a two-dimensional PIC-MCC model already used for standard HTs to calculate the plasma properties in the new configuration. Calculation results exhibit similar behavior than for standard HT, with a predator-prey phenomenon responsible for discharge current oscillations in the range of few tens of kHz. The overlap between ionization and acceleration regions leads to a maximum of ion velocity lower than the one expected. An azimuthal instability responsible for electron transport has also been obtained. The amplitude of azimuthal fluctuating electric field seems too low to explain electron transport by pure stochastic effects as already observed for standard HTs, but more work is needed.

From an experimental point of view, more work is now necessary to characterize the plume of the thruster, especially divergence. The optimization of the thruster design is also studied [29]. Concerning PIC simulations, parametric studies are now underway changing discharge parameters (xenon mass flow, discharge voltage, and magnetic field profiles).

Acknowledgments

This work is supported by the French joint research program GIS "Propulsion par Plasma dans l'Espace". Julien Vaudolon benefits from a CNES-Snecma Ph.D. grant. Access was granted to the HPC resources of CALMIP under the allocation 2013-P1125.

References

[1] S. Y. Cheng and M. Martinez-Sanchez, *Journal of Propulsion and Power* **24**, 987 (2008).

[2] J. Bareilles, G. J. M. Hagelaar, L. Garrigues, C. Boniface, J. P. Boeuf, and N. Gascon, *Physics of Plasmas* **11**, 3035 (2004).

[3] L. S. Mason, R. S. Jankovsky, and D. H. Manzella, "1000 Hours of Testing on a 10 Kilowatt Hall Effect Thruster", *Proceedings of the 37th AIAA Joint Propulsion Conference,* Salt Lake City, UT, paper AIAA-2001-3773 (2001).

[4] S. Mazouffre, G. Bourgeois, J. Vaudolon, L. Garrigues, C. Hénaux, D. Harribey, R. Vilamot, A. Rossi, S. Zurbach, and D. Le Méhauté, "Development and Testing of a Hall Thruster with a Flexible Magnetic Configuration," *Journal of Propulsion and Power* (to be published).

[5] S. Mazouffre, J. Vaudolon, G. Largeau, C. Hénaux, A. Rossi, and D. Harribey, *IEEE Transactions on Plasma Science* **42**, 2668 (2014).

[6] I. G. Mikellides, I. Katz, R. R. Hofer, and D. M. Goebel, *Applied Physics Letters* **102**, 023509 (2013).

[7] I. G. Mikellides, I. Katz, R. R. Hofer, and D. M. Goebel, *Journal of Applied Physics* **115**, 043303 (2014).

[8] R. R. Hofer, D. M. Goebel, I. G. Mikellides, and I. Katz, *Journal of Applied Physics* **115**, 043304 (2014).

[9] S. Mazouffre, S. Tsikata, and J. Vaudolon, *Journal of Applied Physics* **116**, 243302 (2014).

[10] S. Mazouffre, G. Bourgeois, K. Dannenmayer, and A. Lejeune, *Journal of Physics D: Applied Physics* **45**, 185203 (2014).

[11] C. Birdsall and A. Langdon, *Plasma Physics Via Computer Simulation* (IOP, 1998).

[12] R. Hockney and J. Eastwood, *Computer Simulation Using Particles* (Mac Graw-Hill, 1981).

[13] A. Kuzmin, M. Luisier, and O. Schenk, *Fast Methods for Computing Selected Elements of the Green's Function in Massively Parallel Nanoelectronic Device Simulations*, F. Wolf, B. Mohr, and D. an Ney (Eds.), Springer-Verlag Berlin Heidelberg, pp. 533–544, 2013.

[14] C. Petra, O. Schenk, M.Lubin, K. Gaertner, *SIAM Journal on Scientific Computing* **36**, C139-C162 (2014).

[15] H. Liu, B. Wu, D. Yu, Y. Cao, and P. Duan, *Journal of Physics D: Applied Physics* **43**, 165202 (2010).

[16] G. Fubiani, G. J. M. Hagelaar, J. P. Boeuf, and S. Kolev, *Physics of Plasmas* **19**, 043506 (2012).

[17] J. P. Boeuf, B. Chaudhury, and L. Garrigues, *Physics of Plasmas* **19**, 113509 (2012).

[18] J. C. Adam, A. Héron, and G. Laval, *Physics of Plasmas* **11**, 295 (2004).

[19] A. Ducrocq, J. C. Adam, A. Héron, and G. Laval, *Physics of Plasmas* **13**, 102111 (2006).

[20] P. Coche and L. Garrigues, *Physics of Plasmas* **21**, 023503 (2014).

[21] F. I. Parra, A. Ahedo, J. M. Fife, M. Martinez-Sanchez, *Journal of Applied Physics* **100**, 023304 (2006).

[22] S. Barral, K. Makowski, Z. Peradzynski, N. Gascon, and M. Dudeck, *Physics of Plasmas* **10**, 4137 (2003).

[23] S. P. Gary and J. J. Sanderson, *Journal of Plasma Physics* **4**, 739 (1970).

[24] S. P. Gary and J. J. Sanderson, *Journal of Plasma Physics* **4**, 753 (1970).

[25] S. Tsikata, N. Lemoine, V. Pisarev, and D. Grésillon, *Physics of Plasmas* **16**, 033506 (2009).

[26] C.F.F. Karney, *Physics of Fluids* **21**, 1584 (1978); *ibid* **22**, 2188 (1979).

[27] J. Pérez-Luna, « Modélisation et Diagnostic d'un Propulseur à Effet Hall », Thèse de l'Université Paul Sabatier (2008), in French.

[28] J. P. Boeuf, *Frontiers in Physics* **2**, 74 (2014).

[29] S. Mazouffre, J. Vaudolon, and S. Tsikata, "Optimization of the Design of a Wall-Less Hall Thruster", *34th International Electric Propulsion Conference*, Kobe-Hyogo, Japan, paper IEPC-2015-182 (2015).